Highly flexible, green luminescent down converting and hydrophobic 0-D cesium lead bromide (Cs4PbBr6)/ poly (vinylidene difluoride) polymer nanocomposites for photonics and display…

Article *in* Inorganic Chemistry Communications · November 2023

DOI: 10.1016/j.inoche.2023.111761

CITATIONS
3

READS
41

9 authors, including:

Shivaprasad Nagappa
Sri Jayachamarajendra College of Engineering
11 PUBLICATIONS **23** CITATIONS
SEE PROFILE

Bs Madhukar
JSS Science and Technology University, Mysuru
52 PUBLICATIONS **306** CITATIONS
SEE PROFILE

Rajanna Kavya
Sri Jayachamarajendra College of Engineering
8 PUBLICATIONS **10** CITATIONS
SEE PROFILE

Pradeep Reddy Vanga
Vel Tech Rangarajan Dr. Sagunthala R&D Institute of Science and Technology
31 PUBLICATIONS **346** CITATIONS
SEE PROFILE

Inorganic Chemistry Communications 159 (2024) 111761

Contents lists available at ScienceDirect

Inorganic Chemistry Communications

journal homepage: www.elsevier.com/locate/inoche

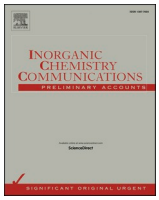

Short communication

Highly flexible, green luminescent down converting and hydrophobic 0-D cesium lead bromide (Cs_4PbBr_6)/ poly (vinylidene difluoride) polymer nanocomposites for photonics and display applications

Nagappa Shivaprasad [a], Mysore Guruswamy Veena [a], Beejaganahalli Sangameshwara Madhukar [b,*], Rajanna Kavya [b], K. Sarath [b], Pradeep Reddy Vanga [c], Geoge Sahaya Dennish Babu [d], Bhagyashree Mahesha Sachith [e], Anjanapura Venkatarmanaiah Raghu [f,*]

[a] Department of Electronic and Communication Engineering, Sri Jayachamarajendra College of Engineering, JSS Science and Technology University, Mysuru 570 006, India
[b] Department of Chemistry, Sri Jayachamarajendra College of Engineering, JSS Science and Technology University, Mysuru 570 006, India
[c] Department of Physics, Vel Tech Rangarajan Dr. Saguntala, R & D Institute of Science and Technology, Chennai 600 062, India
[d] Department of Physics, Chettinad College of Engineering and Technology, Gandhigramam 639 114, India
[e] RIKEN Center for Emergent Matter Science (CEMS), Wako, Saitama 351-0198, Japan
[f] Faculty of Science and Technology, BLDE (Deemed-to-be University), Vijayapura, 586103, Karnataka, India

ARTICLE INFO

Keywords:
PVDF
Cs_4PbBr_6
Nanocomposites
Photoluminescence
PL lifetime decay

ABSTRACT

Halide perovskite materials have emerged as a promising new research topic in recent years, with potential applications in solar cells and optoelectronic devices, among others. These materials have significant limitations, including instability to water, heat, UV radiation, and light, limiting their research to the lab scale only. Encapsulation of perovskite with polymers is a solution for addressing the shortcoming of stability. This study illustrates the synthesis of zero-dimensional cesium lead bromide (Cs_4PbBr_6), as well as its poly (vinylidene difluoride) (PVDF) nanocomposites, optical, morphological, cell properties and increased stability towards the environmental stress. Different concentrations of synthesized perovskite was encapsulated in PVDF, namely 0.0, 0.5, 1.0, 1.5 and 2.0 wt/wt%. The UV–Visible spectral result depicts that the strong absorbance band ranges from 280 to 320 nm confirms the formation of Cs_4PbBr_6. X- ray diffraction (XRD) reveals the existence Cs4PbBr$_6$ and good interaction between the perovskite and polymer matrix. The size of prepared perovskite is in nano scale and with high phase purity with rhombohedral unit cell with are depicted by using high-resolution transmission electron microscope (HR-TEM), selected area electron diffraction (SAED). The nanocomposites exhibit emission from 490 to 520 nm, and 2 wt/wt% of perovskite in PVDF exhibits the highest emission intensity analyzed using photoluminescence (PL) spectral results which is excited at 370 nm. PL lifetime decay measurements of the fabricated PVDF perovskite nanocomposites shows 34.744 ns for 2 % Cs_4PbBr_6/PVDF nanocomposites due to delayed exciton radiative recombination which infers that the fabricated nanocomposites finds potential application in the arena of photonics, UV-radiations blockers, and LEDs.

1. Introduction

All-inorganic perovskite nanoparticles are currently the focus of extensive research in the area of optoelectronic materials. To correlate the optical properties of perovskites with their atomic arrangements a large amount of focus is diverted towards their dimensional and phase control synthesis. In late 1990 [s], all inorganic zero-dimensional lead halide perovskite (LHPs) was first synthesized and reported more stable photoluminescence quantum yield (PLQY)[1]. The phase pure crystalline structure of Cs_4PbBr_6 is devoid of corner shared octahedra $[PbBr_6]^{4-}$ leading to increase in the quantum confinement of the photo excited excitons than that of the $CsPbBr_3$. Owing to the above reason Cs_4PbBr_6

* Corresponding authors.
E-mail addresses: madhukarbs007@jssstuniv.in (B.S. Madhukar), gsraghu2003@yahoo.co.in (A.V. Raghu).

https://doi.org/10.1016/j.inoche.2023.111761
Received 19 July 2023; Received in revised form 12 November 2023; Accepted 16 November 2023
Available online 24 November 2023

phase is usually called a Zero-Dimensional Perovskite (0-D). Soon after 2016 due to rapidly increasing interest, LHPs and other metal halides along with Cs_4PbBr_6 compound works began to report with excellent and firm green photoluminescence [2].

In recent years, perovskite nanoparticles have emerged as an extremely important material for a range of applications, including light-emitting diodes (LEDs), solar cells, lasers, and photodetectors. Despite the fact that it boosts remarkable optical properties, it is plagued by a number of challenges, the most significant of which are poor stability under external stress mainly thermal stability, photo stability, resistance to water, and anion exchange[3]. From past decade many investigations have been reported stating the synthesis of different types of perovskites including all inorganic and organic perovskites structures and evaluated their photovoltaic performance.Murugadoss et al. [4], Murugadoss et al. [5],Murugadoss et al. [6].

To employ for technological applications, enhancing the stability of the perovskite is of great importance which in turn enhances the life span of end devices [7]. Various chemical routes have been suggested to improve stability of the lead halide perovskites by combining them with suitable class of materials such as carbon-based nanomaterials (Graphene & other 2D materials)[8], metal and non-metal nanomaterials (silica and alumina)[9]and organic polymers[10]. Polymers are the most commonly used material to encapsulate and to embed the LHPs and inorganic nanofillers to increase the stability of the aforesaid.

Polymeric nanocomposites possess superior mechanical, thermal and electrical properties than that of conventional micro sized filler composites due to the ultrafine dimension of the filler. These enhanced properties are attributed due to the large interfacial area of the nanoparticles. In recent years, polymer nanocomposites, especially with metallic nanofillers particularly with metal oxidesRamesan et al. [11], Sankar et al. [12],Ramesan et al. [13],Ramesan et al. [14],Ramesan et al. [15], have attracted much attention for use in electrical applications due to encouraging results obtained for their dielectric properties. These materials are both inorganic and organic polymer nano hybrids, with optical, electrical, and optoelectronic capabilities that are widely employed in optical applications such as lenses, optical waveguides, optical switches, light emitting diodes, nonlinear optical devices and photonics[16].

Using ligand-assisted re-precipitation, Xiao and his colleagues produced water-stable Poly(methyl)methacrylate (PMMA) perovskite nanocomposites with reduced surface flaws. The link between perovskites' Pb and PMMA's carbonyl group hinders H_2O diffusion, making perovskites PMMA nanocomposites resistant to aqueous medium and temperature.[7]. Macroscale polymer encapsulation improves light, water, and PLQY stability and can tolerate $>$ 1010 photons per QD. Perovskite QDs' hydrophobic surface coating and polymers may preserve light stability and quantum yield following water exposure. Ligand-hydrophobic polymer matching helps bulk and thin film perovskites resist lead leakage in optical devices like optically-pumped lasers and polarized downshifters.[17].

Polymers, which have strong chemical stability and powerful resistance to oxidation and corrosion, are a promising choice for combining these with perovskites to improve their stability. Despite their numerous favorable attributes, they have poor stability concerns with oxygen, moisture, heat, and radiation, which restricts their practical applicability. Over the past several years, a series of experiments has been conducted in attempt to improve the stability of perovskite.

PVDF, a piezoelectric polymer, was excellent for flexible nanogenerators. The most common and thermodynamically stable phase is the non-electroactive β-phase, however electroactive and β-phases are desired. PVDF electroactive phases are usually promoted by mechanical stretching and electrical poling. Because of its chemical stability, mechanical resistance, dimensional stability, and biocompatibility, the flexible PVDF polymer might be a nanogenerator in self-powered flexible electronic devices. PVDF, an electroactive polymer, is also used in sensors, actuators, and energy harvesting systems.[18].From past decade great number of research investigations have been carried out on PVDF/metal oxide nanocomposites to explore the optical, thermal and electrical properties which leads their optoelectronic applications. Alhassan et al. [19],Alhassan et al. [20],Taha and Mahmoud [21],Taha et al. [22], Lovinger, A. J., [23], Liu, Y. et al [24].

Michaela Meyns and his team developed a unique coating method that improved the chemical and optical stability of perovskite nanocrystals (NC). Poly (maleic anhydride-alt-1-octadecene) (PMA) is used to synthesize perovskite NCs. The selection of emission wavelengths and small emission bandwidths of these NCs allowed the creation of color conversion LEDs with high radiation efficacies and rich colors. [10]. Juan He et al. employed polystyrene (PS), polycarbonate (PC), and acrylonitrile butadiene styrene (ABS) for microencapsulation and methyl ammonium bromide as perovskite to make polymer-perovskites. Ultrastable and luminescent narrow green emission band perovskite-polymer composite films are made. Such films may be used with blue LEDs and red downconverters including red CdSe-based QDs, potassium Silicon Fluoride phosphor, and two hybrid BLU setups to provide an 89 to 91 % color range (Juan [25].

A facile, affordable co-polymer templated synthesis approach for stable photo-stable core–shell colloidal perovskite NC was developed recently [Xi, L., et al] [28]. The hydrophobic polymer shell excludes polar liquids. In colloidal and thin film forms, multi-dentate core/shell perovskite NC is orders of magnitude more stable[26]. 1D-2D $CsPbBr_3$/PMMA nanocomposites were fabricated by using scale-up synthesis of fluorescent perovskite nanocrystals using $CsPbBr_3$ PNCs/PMMA composites with PL stability at room temperature by means of microfluidic spinning. This work provided a greener way to mass produce perovskite NC composite materials with excellent fluorescence and stability for optoelectronics [27]. $CsPbCl_3$ perovskite quantum dots (PQDs) in PMMA layers have been used to develop the memory devices with increased memory stability. These findings help investigate PQD-doped organic memory [29].

The above literature survey shows that there are several research works progressing, to demonstrate the use of perovskite polymer nanocomposites to enhance the stability of the perovskite and helps in widening the application window. Here we present a novel report, of utilizing the PVDF for encapsulation of the 0-D perovskite and to evaluate their optical property and stability towards the environmental stress.

2. Materials and methods

2.1. Materials

Cesium bromide (CsBr) (99.9 %), lead bromide ($PbBr_2$) (99.9 %), oleylamine (70 %), oleic acid (90 %), toluene (99.8 %), 1-octadecene, N, N-dimethylformamide (DMF) and poly (vinylidene difluoride) ($M_w \sim$ 180000). These chemicals are procured from Sigma Aldrich and were used without any purification and treatment.

2.2. Characterization

The obtained Cs_4PbBr_6, Cs_4PbBr_6/PVDF nanocomposite morphology are studied using SEM Joel IT-300 (Japan). The phase purity and the crystal structure were confirmed by studying XRD profile of the as obtained Cs_4PbBr_6, Cs_4PbBr_6/PVDF NCs using PROTO AXRD benchtop (Canada) with the dwell time of 0.2 s. HRTEM and SAED techniques were used to identify the morphology and phase purity of the prepared perovskite Thermo fisher, Talos F200 S, (USA). UV–Visible absorption spectra of as synthesized perovskites and its PVDF nanocomposites were carried out using shimadzo 1900, (Japan) spectrophotometer with slow scan rate. Steady-state PL spectra were acquired on a HORIBA FL3 spectrofluorometer with 370 nm photoexcitation from a Xe arc lamp. Transient PL decay measurements were performed by time-correlated single-photon counting on a HORIBA FL3 spectrofluorometer with a

370 nm LED pump source (pulse width < 1.2 ns). Contact angle meter (HO: IADCM-081, India) was used to measure the contact angle and surface energy.

2.3. Synthesis of Cs_4PbBr_6 by re-precipitation method

In a typical synthesis of Cs_4PbBr_6, $PbBr_2$ (0.2 mmol) and CsBr (0.2 mmol) are initially dissolved in 5 mL of DMF (solvent). Then 2.5 mL of oleic acid and 1.25 mL oleylamine are added to the above prepared solution at the room temperature. Further 0.4 mL of this precursor solution was quickly added into 10 mL of toluene which acts as a bad solvent, under vigorous stirring for about 30 mins at room temperature. A bright yellowish green color was observed instantaneously after the addition of the above solution to toluene. This indicates the formation of 0-D Cs_4PbBr_6 and it is being confirmed through XRD, SEM with EDAX (**Fig. S1**).

2.4. Fabrication of Cs_4PbBr_6/PVDF perovskites nanocomposites

The various composition *viz.*, 0, 0.5, 1, 1.5 and 2 (Wt/Wt%) (<2% the perovskite is gets agglomerated and oozing out of the polymer) of Cs_4PbBr_6/PVDF nanocomposites were fabricated using simple solvent casting method. The calculated amount of above prepared perovskite was weighed and added to the 2 % PVDF solution which was dissolved in DMF. The prepared solution is stirred well at room temperature using magnetic stirrer to get uniform distribution. Later the composites were casted in a clean glass mould and the solvent was allowed to evaporate completely without disturbing the mould at 45–50 °C. After the complete evaporation of the solvent, the films were carefully removed from the mould and the obtained nanocomposites films having thickness in the range of 0.23–0.35 mm, which is subjected for various characterizations (**Fig. S2**).

3. Results and discussion

3.1. Wide angle X-ray scattering spectroscopy (WAXS)

Microstructural characteristics and phase purity of Cs_4PbBr_6 NP is examined using WAXS. The phase profile of the synthesized Cs_4PbBr_6 perovskite are presented in Fig. 1 **(a)**. The XRD pattern with the peak centred at 2θ = 12.6, 20.1, 22.5, 25.4, 27.6, 28.7, 30.3, 31.1, 34.7, 39.0, 45.9, 45.7 and 58.5° corresponds to the crystal plane diffraction from (1 1 0), (1 1 3), (3 0 0), (0 2 4), (1 3 1), (2 1 4), (2 2 3), (0 0 6), (1 3 4), (3 3 0), (6 0 0) and (7 0 4) of Cs_4PbBr_6 corresponds for rhombohedral unit cell. To further confirm the rhombohedral unit cell, XRD data obtained for the synthesized perovskite is utilized for the theoretical studies by using rietveld profile and integrated intensity refinement were performed by Fullprof software. Fig. 1**(b)** shows the rietveld refinement of the synthesized Cs_4PbBr_6. From the data obtained it is clear that the obtained perovskite is having rhombohedral crystallographic unit cell with the space group of *R-3c* having the lattice parameter of a = b = 13.70 Å and c = 17.28 Å, that is typically formed by octahedral $(PbX_6)^{-4}$ clusters separated by Cs^+ ions which confirms the presence of Cs_4PbBr_6 (Fig. 2) [30,31].

X-ray diffraction was carried out further to investigate the effect of Cs_4PbBr_6 inclusion on the microcrystalline parameters and the interaction between PVDF. From the XRD profile (Fig. 3) it is clear that the perovskite and the polymer exhibits good interaction. Also in XRD profile, polymer and its perovskite composites possess the peak corresponding to the β- phase of the PVDF with the 2θ centered from 19.80°-20.59°[32]. The XRD peak of pure polymer does not show any peaks corresponds to the perovskite, whereas after inclusion of Cs_4PbBr_6 new peaks along with PVDF peaks shows its presence, with variation of the intensity corresponding to the β- phase of the polymer which depicts the interaction of the polymer and the perovskite.

To probe the effect of addition of the perovskite to polymer the microcrystalline parameter of the prepared perovskite nanocomposites was evaluated. The computed microcrystalline parameters were tabulated in Table 1. Scherrer lengths or average crystallite size (L) of the nanocomposites was calculated by using Scherrer formula:[33].

$$L = \frac{k\lambda}{\mathrm{Cos}\theta\beta} \quad (1)$$

where, k, λ and θ are the constant (k = 0.9), which is related to the crystallite shape, the radiation wavelength and Bragg's angle, respectively; whereas, β is the full width at half maximum (FWHM) of the diffraction peak. The computed crystalline size of individual nanocomposites is shown in Table 1, which may be accessed on this page. This table demonstrates that the addition of Cs_4PbBr_6 resulted in the formation of elemental vacancies and an increase in the interaction between the filler and the polymer, both of which reduce the lattice properties (Mallikarjuna et al., 2004). The insertion of Cs_4PbBr_6 into PVDF prevents the agglomeration phenomena that occur between Cs_4PbBr_6 nanoparticles and also increases the material's crystalline size. It is also noted that the FWHM of the composites decreases with increase in Cs_4PbBr_6 content which gives a positive effect to the crystallite size.

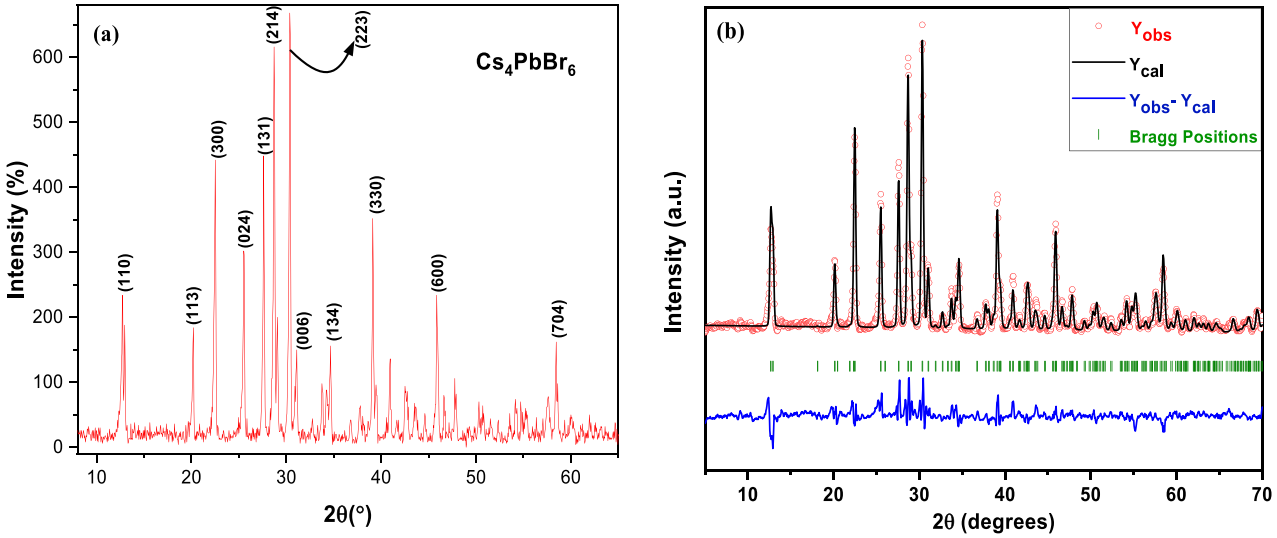

Fig. 1. (a) X-ray diffraction pattern of Cs_4PbBr_6, (b) Rietveld refinement of Cs_4PbBr_6.

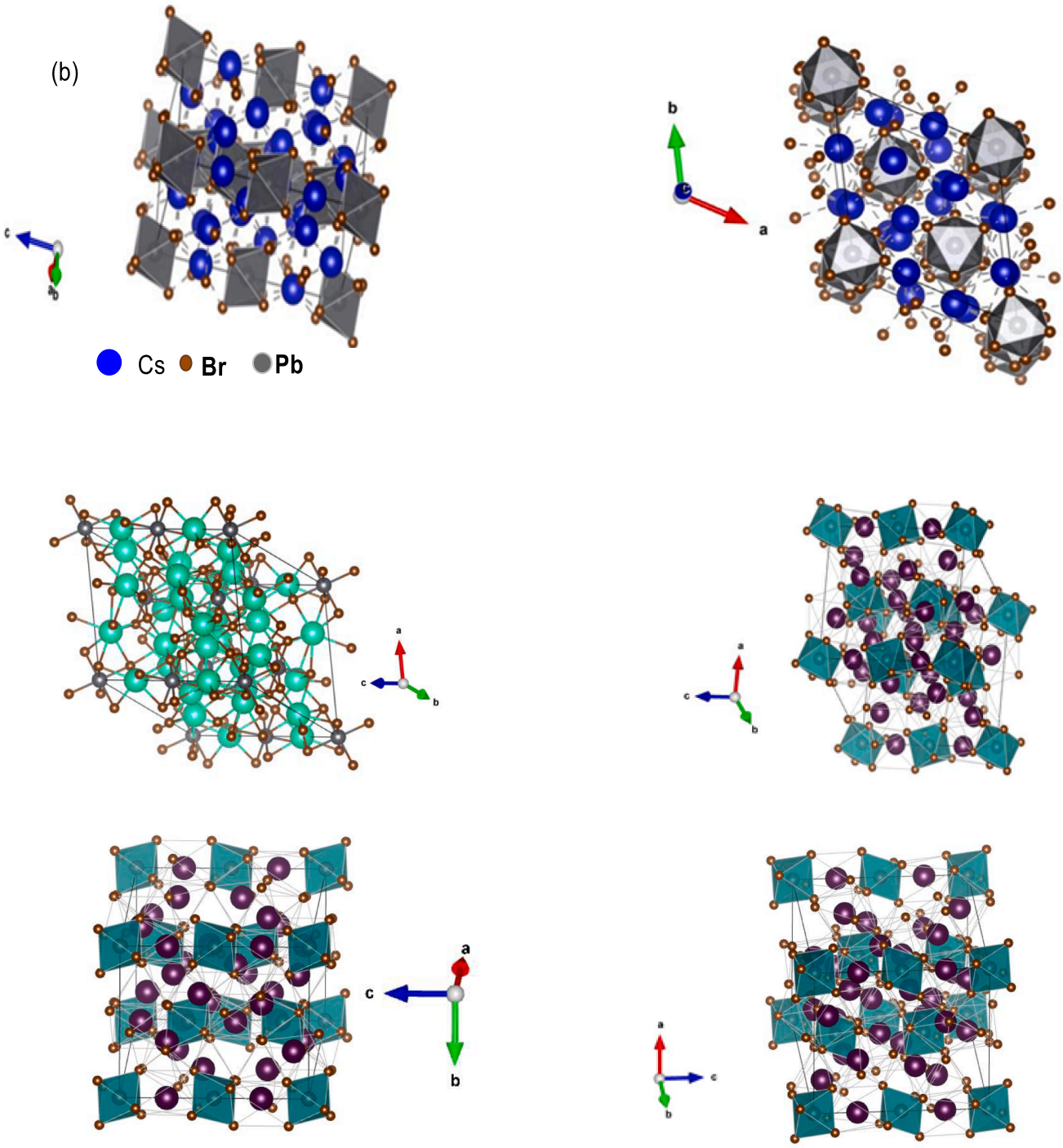

Fig. 2. Crystal packing structure of Cs_4PbBr_6 at different orientation.

Furthermore, the variation of the Cs_4PbBr_6 content also effects the nature of the XRD profile which is less intense and much broader when compared to plain PVDF. This characteristics of the peaks can be attributed for the decreased intermolecular chain interaction between the polymeric chains due the presence of the Cs_4PbBr_6 at the interface (Nataraj et al., 2008). It is responsible for the variation in the interplanar distance (d-spacing) which shows the higher values for the nanocomposites when compare to the pristine polymer [33].

In addition, lattice strain and dislocation density were calculated for the 2θ values tabulated in Table 1 and it is clear that as the concentration of the Cs_4PbBr_6 increase, there is corresponding decreases in the lattice strain and dislocation density in the polymer matrix resulting in decreases in the structural disorder in the PVDF matrix. Thus, the crystalline nature of nanocomposites increases with increase in Cs_4PbBr_6 concentration in the PVDF matrix [32].

3.2. Transmission electron microscope (TEM) and selected area electron diffraction (SAED)

To evaluate the particle size and the type of crystallite nature TEM and SAED analysis is employed. The results obtained from the TEM and SAED analysis are showed in Fig. 4. From the TEM images Fig. 4 **(a) & (b)** it is cleared that the perovskites exhibit the size in the nanometer scale and also hexagonal shaped structure which can be observed in

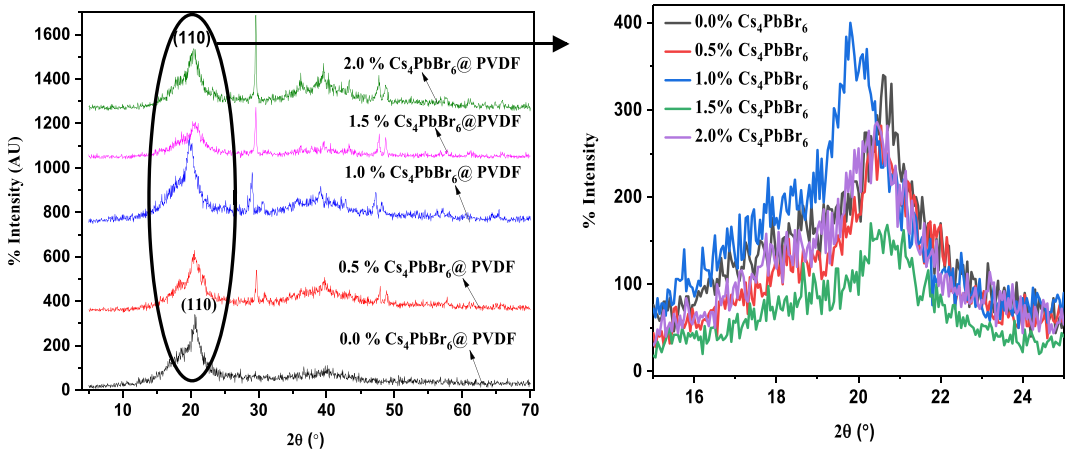

Fig. 3. XRD profiles of PVDF/Cs_4PbBr_6 nanocomposites.

Table 1
Microcrystalline parameter of PVDF/Cs_4PbBr_6 nanocomposites.

PVDF/Cs_4PbBr_6 (wt/wt%)	2θ (°)	FWHM (β)	'd' spacing (Å)	Scherrer length (L) (Å)	η x10^{-4}	Lattice strain × 10^{-1}	R	SF
100/00	20.59	1.95	4.30	72.35	1.91	4.79	5.38	1.69
99.5/0.5	20.54	1.88	4.31	74.93	1.78	4.62	5.40	1.93
99.0/1.0	19.80	1.85	4.47	76.30	1.71	4.54	5.59	1.93
98.5/1.5	20.29	1.63	4.37	86.29	1.34	4.01	5.46	1.69
98.0/2.0	20.43	1.43	4.34	98.42	1.03	3.52	5.42	1.47

Fig. 4**c**.[34]. Furthermore, from the images it is also evident that the synthesized perovskite is showing the unidirectional lines (Fig. 4**d**.) owing to the presence of single type of crystallite phase. Confirming that the synthesized perovskite is having high phase purity, rhombohedral, without any mixing of other crystallite phases which is in good agreement with the results obtained for XRD analysis. Fig. 4.(**e and f**) represents the SAED analysis of the prepared perovskite which possess bright spots, representing that the obtained perovskite is phase pure and possessing single type of unit crystal. Furthermore, the EDS (Fig. 5) data shows (Table 2) the presence of Cs, Br and Pb which is nearer to the theoretical data (cesium − 4, bromide-6 and lead −1 number) confirming the obtained perovskite is Cs_4PbBr_6.

3.3. Scanning electron microscope (SEM) analysis

The scanning electron microscope is used to evaluate the microscopic properties of the nanofiller and its polymer nanocomposites. Furthermore, it is also employed to study the effective influence of perovskite on the topological features of the polymer nanocomposites and the extent of dispersion of the perovskite in the host polymer. The scanning electron micrograph images of perovskite and its composites (Figs. 6 and 7) exhibits an excellent dispersion in the polymer host matrix depicting greater compatibility between the perovskite and the polymer, exhibiting the homogeneous distribution of filler in polymer matrix. From the SEM microphotograph it is clear that the perovskite filler is integrated with excellent filler dispersion in addition to noticeable chemical compatibility between the perovskite fractals with the polymer. From Fig. 7 **(a-d)** it is clear that the perovskite added to polymer matrix can be observed clearly with cubic like structure which is absent in pristine polymer, furthermore as the concentration of the perovskite increases form 0 % to 1.5 % the number of the cubes like structures observed also increases. Whereas the perovskite concentration increases to 2.0 % the agglomeration of the fillers in the host polymer matrix is observed clearly in Fig. 7**(d)** indicating the threshold concentration of the perovskite filler. The prepared perovskite is also subjected to SEM analysis and hexagonal shaped structures are cleared observed which is in good agreement with the previously literature, indicating the formation of the 0D Cs_4PbBr_6 [35].

3.4. Optical properties

3.4.1. Uv–visible absorbance studies

The semiconducting nanoparticles in polymer nanocomposites, they are seen as a potential material for electrical and optoelectronic applications. Before to incorporate new material for any optoelectronic device applications, primarily it is affirmed to be optoelectronic in nature. The films were cast with this objective in mind, allowing UV–Visible spectrum studies to be utilized to characterize the optical properties of PVDF nanocomposites containing Cs_4PbBr_6 as nanofillers. The UV–Visible absorbance spectrum of the prepared nanocomposites is presented in Fig. 8. The absorbance spectrum clearly reveals the filler concentration dependent optical properties of PVDF host with first excitonic absorbance showing in ultraviolet region ranging from 280 to 320 nm with λ_{max} of 310 nm (Seth, and Samanta., 2017). This absorption feature in UV regime is consistent with that of bulk Cs_4PbBr_6, which was proven to be the localized $^6S_{1/2}$–$^6P_{1/2}$ transition within the isolated $[PbBr_6]^{4-}$ octahedra separated by Cs^+ ions [36]and also can be attributed π to π* of the double bond present in the polymer back bone (ethylene unsaturation) results in synergetic effect and formation of charge transfer complexes between the polymer-Cs_4PbBr_6 [38]. Owing to this absorbance peaks indicates that the presence of perovskite, which is absent in the pristine polymer[34]. Additionally, the investigated nanocomposites are suitable candidates for UV-Shielding applications due to their extremely high UV absorbance (Kim et al., 2012)[37]. The absorption increases with increasing Cs_4PbBr_6 content, and the shift in the absorption edge of the doped PVDF nanocomposites exhibits the variation in the energy band gap. This may be caused by modifications in the crystallinity of the polymer matrix or the formation of charge transfer complexes [39].

The transmittance of pure PVDF and PVDF/Cs_4PbBr_6 nanocomposites is shown in **Fig. S3** as a function of wavelength. From the graph it is clear that as the concentration of Cs_4PbBr_6 increases, the transmittance of nanocomposites decreases, which is attributed to the increasing Cs_4PbBr_6 layers. Furthermore, any decreasing trend in

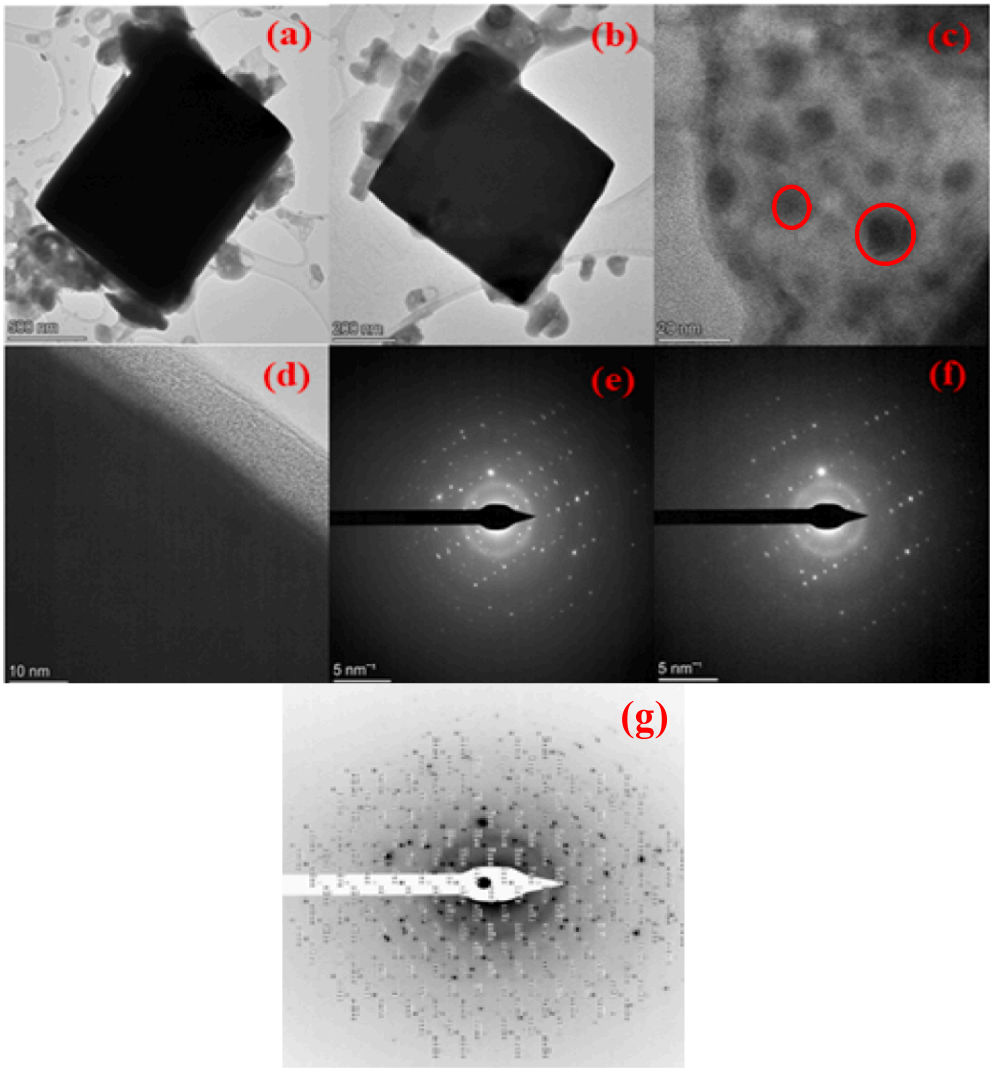

Fig. 4. TEM and SAED micro photographic images of prepared Cs_4PbBr_6.

transmittance observed in the nanocomposite is due to the fact that the Cs_4PbBr_6 nanoparticles present in the nanocomposites involves in scattering and the reflection of incident light decreases the transmittance of the whole nanocomposites. The particle size, dispersion, surface roughness, polymer-filler interface, and refractive index of the additive, along with other physical characteristics, have a significant impact on the transmittance of the resulting nanocomposite [40].

Absorption coefficient (α) is an important parameter which is used to study the absorption edge and type of electronic transition of any materials which in turn finds application in the field of photo detector, light emitting diodes, photovoltaic cells. To evaluate the absorption edge of the prepared perovskite nanocomposites α is computed by absorbance values using the formula.

$$\alpha = \frac{A \times 2.303}{t} \tag{2}$$

where A is the absorption at a specific wavelength and t is the compactness of the film. The absorption edge of the perovskite nanocomposites was obtained by extrapolating the linear portion of the plot of absorption coefficient and photon energy. The obtained values are tabulated in the Table 3 and represented in Fig. 9 **(a)** and [**Fig. S4**]. From the table it is cleared that as the concentration of the perovskite increases there is a monotonic decrease in the absorption edge. Pristine PVDF shows 3.4 eV whereas 2 % Cs_4PbBr_6 doped polymer nanocomposites exhibits 3.1 eV. This monotonic decrease in the absorption edge can be attributed for the effective dispersion of the doped perovskite in the polymer matrix. Furthermore, the absorbance increases noticeably as it approaches near the absorption edge, indicating that the nanocomposites are of good crystalline nature and likely to play a significant role in photodetector research and design [41].

The absorption coefficient so obtained was also employed to find out the type of the transition that takes place in the prepared nanocomposites. The optical band gap for different concentrations of Cs_4PbBr_6/PVDF nanocomposites was resolved using Wood and Tauc's plot. Furthermore, this plot also provides the information about the interaction of polymer and added perovskite nano particles[33]. The E_g can be calculated by using α and the intercept of the extrapolated linear plot of $(\alpha h\nu)^2$ and $(\alpha h\nu)^{1/2}$ *versus* photon energy ($h\nu$) respectively yields the direct and indirect optical band gaps.

$$(\alpha h\vartheta)^{\frac{1}{m}} = B\left(h\vartheta - E_g\right) \tag{3}$$

where m is an index related to the type of electronic transition, with values of 1/2, and 2 for direct allowed and indirect allowed electronic transitions, respectively, and h is the photon energy in eV, Eg is the optical band gap (eV), and α is the absorption coefficient in cm^{-1}Ali and Kadhem [42]. It's been evident from the Table 3 that with increasing concentration of Cs_4PbBr_6 in composites, value of direct band gap (E_{dg}) for 0 to 2 % Cs_4PbBr_6 ranges from 4.64 to 3.17 eV and indirect band gap

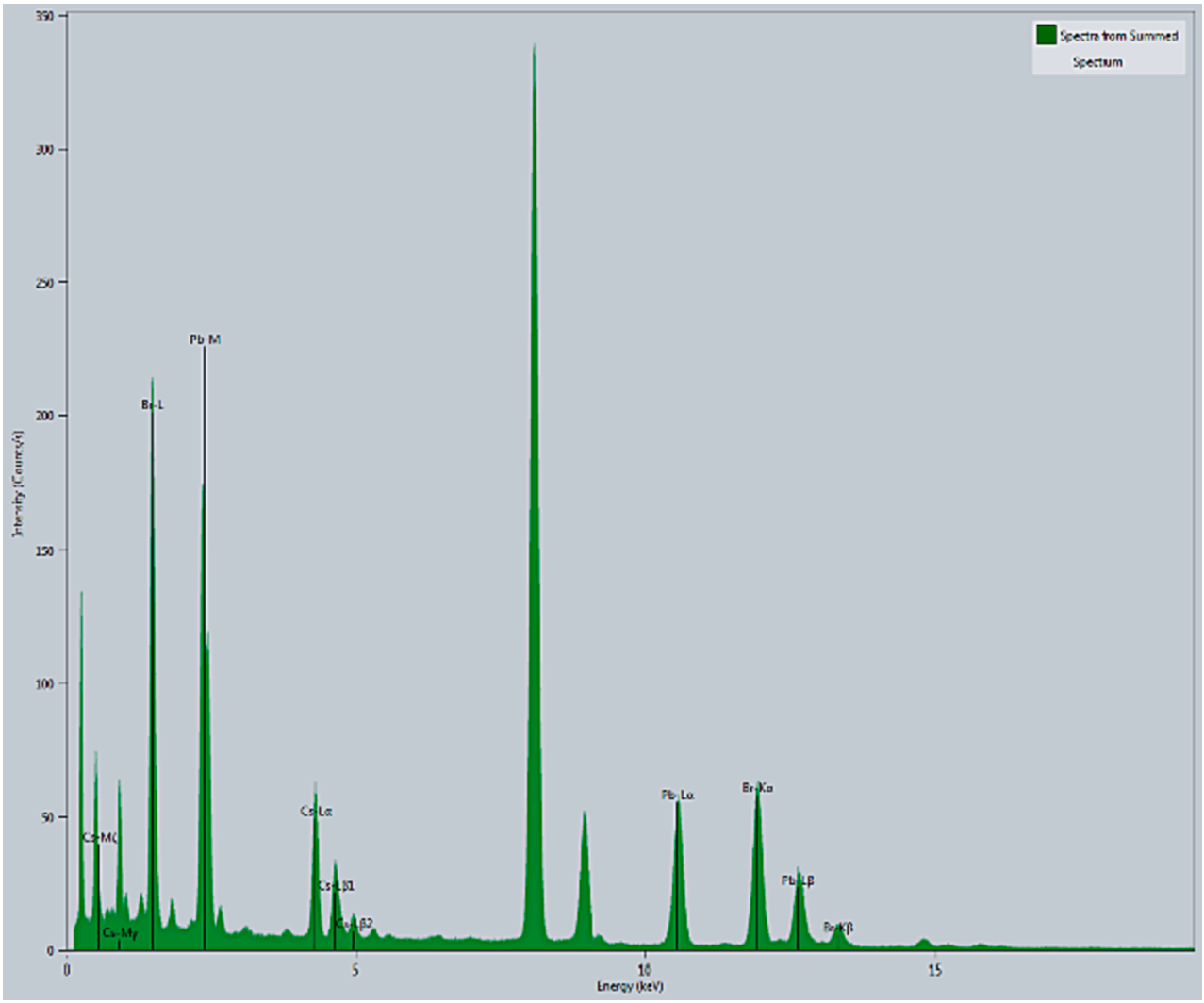

Fig. 5. EDS pattern for the synthesized Cs_4PbBr_6.

Table 2
Elemental composition obtained from EDS of synthesized Cs_4PbBr_6.

Elements	Weight (%)	Atomic (%) X 10	Net intensity X (10^4)	Error	K-ratio
Br	34.8	5.16	5.03	0.268	1.0
Cs	35.0	3. 72	8.42	0.278	0.57
Pb	30.1	1. 12	4.11	0.404	0.98

(E_{ing}) for 0 to 2 % Cs_4PbBr_6 ranges from 3.64 to 2.85 eV shows monotonic decrease. The decrease in the band gap of the nanocomposites is due to the fact that increase in degree of disorder in the PVDF/Cs_4PbBr_6 nanocomposites, chemical and physical conjugation of the Cs_4PbBr_6 nanoparticles with the PVDF, which allows the coupling of possible electronic states of the dopant and the polymer host results in generation of new lower electronic transition energy state within the polymeric band gap. The emergence of a new transitional level below the conduction band was held responsible for the narrowing of the optical band gap for PVDF/Cs_4PbBr_6 nanocomposite (2.0 %) [[43,44,45]. Furthermore, from the Fig. 10 (a) (**Fig. S5**) it is observed that the plot is linear over wide range of photon energy and at the m = 2 the curve gets intercepts with a value of zero, whereas for m = 1/2 will not take place which indicates the direct type of transition which is in good agreement with the work published by Saif M.H. Qaid et al[46].

The Urbach rule can be used to explain how the absorption coefficient near the band edge exhibits an exponential relationship with photon energy.

$$\alpha = \alpha_0 \exp(E - E_u) \quad (4)$$

The localized states band tail energies E_u in the optical gap can be calculated using this relation (Eq. (4). Fig. 10**(b)** depicts the variation of ln (α) against photon energy (eV) for PVDF@Cs_4PbBr_6 nanocomposites at various concentrations of Cs_4PbBr_6. The slope of the straight lines forming these curves was used to calculate the values of E_u, which are shown in Table 3 Urbach [47]. The relationship between E_u values and dopant content is shown to be monotonic increase with the increase in dopant concentration ranging from 0.17 to 0.71 eV infers the dependence of the absorption coefficient with photon energy. Furthermore, from the table it is also clear that the incorporated Cs_4PbBr_6 nanoparticles alter the structure of the host PVDF polymer matrix due to the molecular ordering in nanocomposites causes an increase in the number of charge trapping centers Santhosh et al. [48].

Refractive index (RI) and efficiency are the two factors that most strongly influence the effectiveness of solar cells. It is well known fact that solar cells on a large scale require a high refractive index[49]. RI for semiconducting materials is also important as it alters the optical and electrical properties of the materials and gives the knowledge about to which application the material can be applied.

The refractive index (n) of the PVDF/Cs_4PbBr_6 is computed by using Fresnel formula:

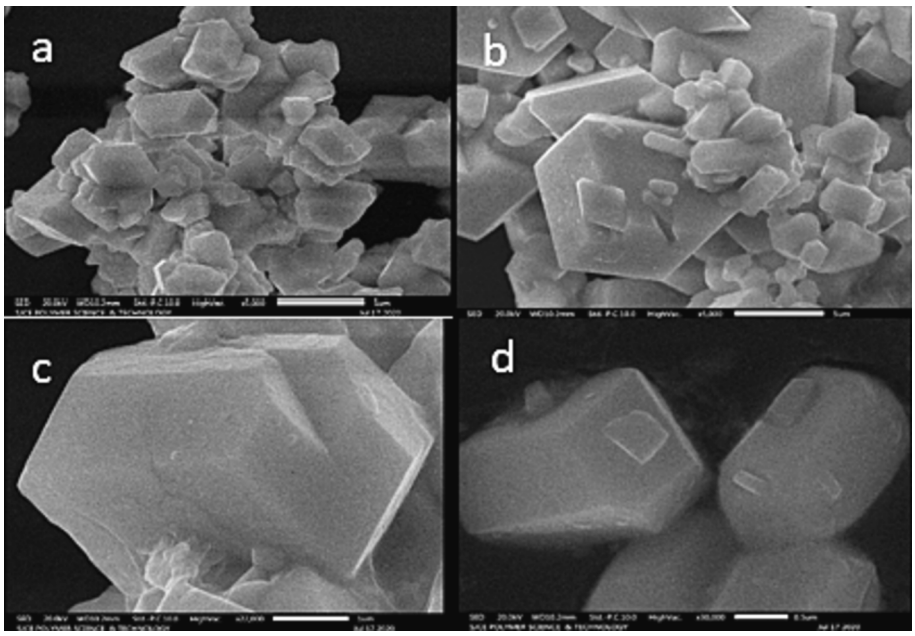

Fig. 6. Scanning electron microscopic images of Cs_4PbBr_6.

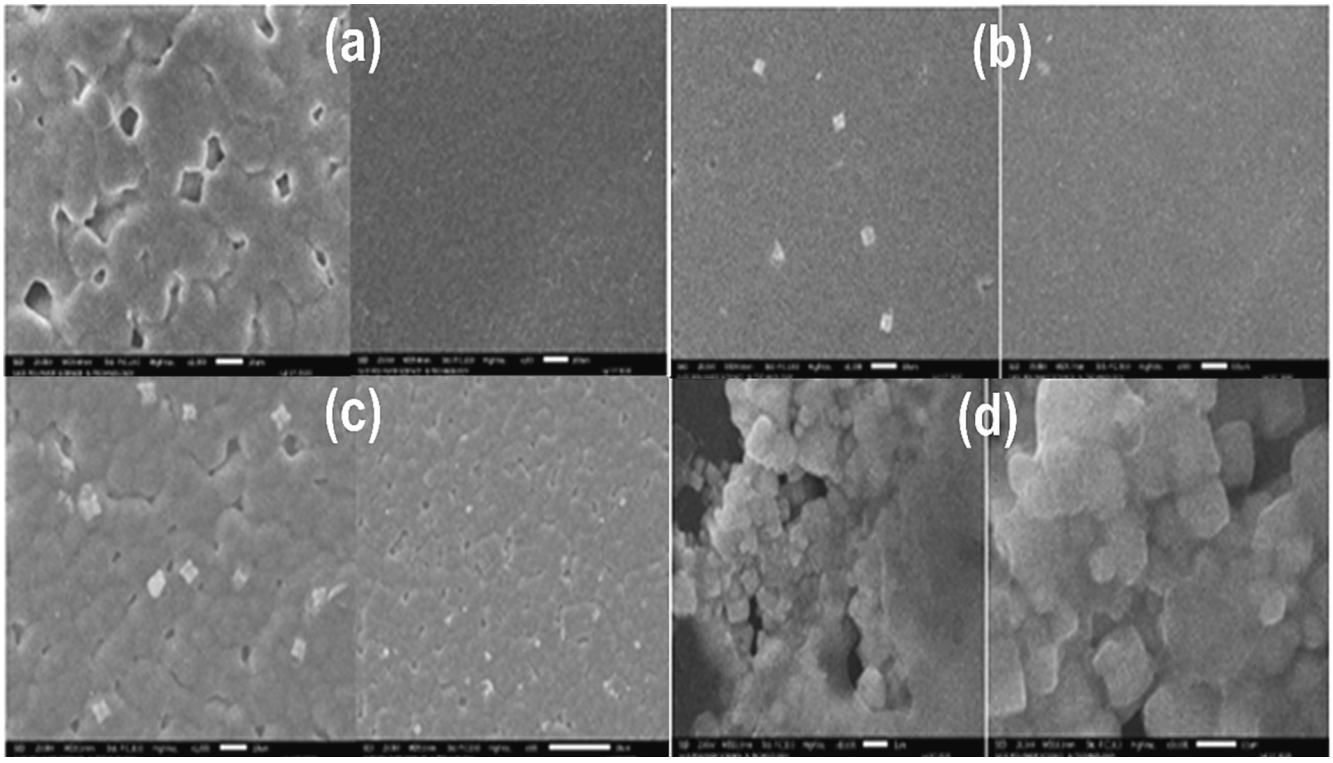

Fig. 7. Scanning electron microscopic images of (a) 0.0% (b) 1.0, (c) 1.5%, and (d) 2.0% Cs_4PbBr_6 /PVDF nanocomposites.

$$n = \left(\frac{1+R}{1-R}\right) + \left(\frac{4R}{1-R^2} - K^2\right)^{\frac{1}{2}} \quad (5)$$

where, n is refractive index, R is reflectance, K is extinction coefficient it is calculated by following equation.

$$K = \frac{\alpha\lambda}{4\pi} \quad (6)$$

According to Bhar and Pinto models, the n values increases with increase in the nano filler concentration due to net atomic refractions, low density, large surface area, and high absorption coefficient. The refractive index rises from 48.5 for pure PVDF to 49.2 for PVDF/2% Cs_4PbBr_6, as seen in **Fig. S6** and the values are tabulated in Table 3. The increased packing density of the polymer is correlated with the rise in refractive index. It is evidenced that the UV region perceives a significant drop in the extinction coefficient (k). As Cs_4PbBr_6 concentration in the polymer matrix rises, the absorption peak of Cs_4PbBr_6 is clearly visible and the extinction coefficient rises on the higher wavelength region. This is due to the increase in packing density of polymers. This

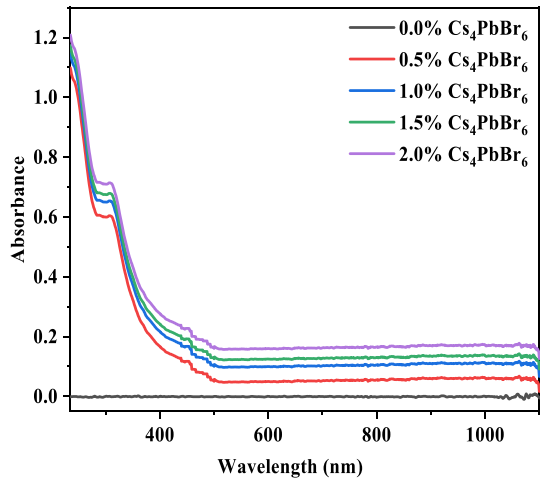

Fig. 8. UV–Visible absorption spectra of PVDF/Cs_4PbBr_6 nanocomposite.

reveals that as Cs_4PbBr_6 levels increases, the amount of light lost due to scattering and absorption also increases (N. Kundachira Subramani, et al., 2015) [50]. From this relationship, it is clear that the fabricated nano composite becomes more and more opaque when filler quantity and particle size are increased. However, the high refractive index transparent polymer composites with high visible transparencies may be achieved by using an ideal volume fraction of filler with filler size within 20–40 nm fraction and near matching inorganic filler to organic matrix RI.

Extension coefficient (K) is regarded as the imaginary part of the multipart refractive index and mainly recedes on absorption coefficient (α) and wavelength (λ) which are related and computed by using the equation (5) and the obtained results are presented in **Fig. S7** (Table 3). K is a parameter which quantifies the amount of photonic energy that get relieved due to the specific scattering and absorption by the prepared nanocomposites. **Fig. S7** shows the variation of K with respect to wavelength (λ). The extinction coefficient increases as the wavelength raises to higher value. The surface Plasmon resonance of Cs_4PbBr_6 may account for the sharp rise in extinction coefficient > 510 nm. The scattering process of incoming light, in which the energy of photons decreases, is responsible for the rising K values at shorter wavelengths than 510 nm.

3.4.2. *Photoluminescence spectroscopy*

PL spectroscopy is an appealing technology that can analyze the structure and features of materials with great accuracy at the nanoscopic level and with remarkable sensitivity. PL spectroscopy is one of the important tool to differentiate between Cs_4PbBr_6 and $CsPbBr_3$. The prepared zero dimensional Cs_4PbBr_6 can be confirmed by employing PL spectroscopy. The synthesized perovskite is characterized by PL spectra and the obtained result is presented in Fig. 11**(a)**. From the Fig. 11, it is clear that the synthesized perovskite shows small amount of impurities with strong emission peak ranging from 450 to 550 nm with λ_{max} of 510 nm which confirms that the prepared perovskite is Cs_4PbBr_6 and not $CsPbBr_3$. Furthermore, the full width half maximum (FWHM) of the peak obtained shows a narrow value of 22 nm further conforming that the obtained perovskite is Cs_4PbBr_6 [51].

Noticeable flattening of the valence and conduction bands is seen when transitioning from the 3D to the 0D perovskite, which is in agreement with the observation of an ensuing widening of the bandgap upon reducing the structural dimension. In all three situations, Pb-6p and Br-4p states predominate in the conduction band minimum (CBM) or lowest unoccupied molecular orbital, (LUMO), whereas Pb-6 s and Br-4p states make up the valence band maximum (VBM) or highest occupied molecular orbital (HOMO). The electronic zero-dimensionality of the structure of 0D perovskites is primarily responsible for the high

Table 3
Optical properties of plain PVDF and PVDF/Cs_4PbBr_6 nanocomposites.

PVDF/ Cs_4PbBr_6 (wt/wt%)	E_g (Direct) (eV)	E_g (Indirect) (eV)	Urbach Energy (E_u)	Absorption edge	Refractive Index (10^1)	Extension Coefficient (10^4)
100/0.0	4.69	3.64	0.43	3.40	48.50	2.24
99.5/0.5	3.34	3.07	0.44	3.28	48.90	3.23
99.0/1.0	3.29	3.02	0.49	3.17	49.00	4.19
98.5/1.5	3.23	2.95	0.54	3.11	49.14	4.71
98.0/2.0	3.17	2.85	0.71	3.05	49.20	5.48

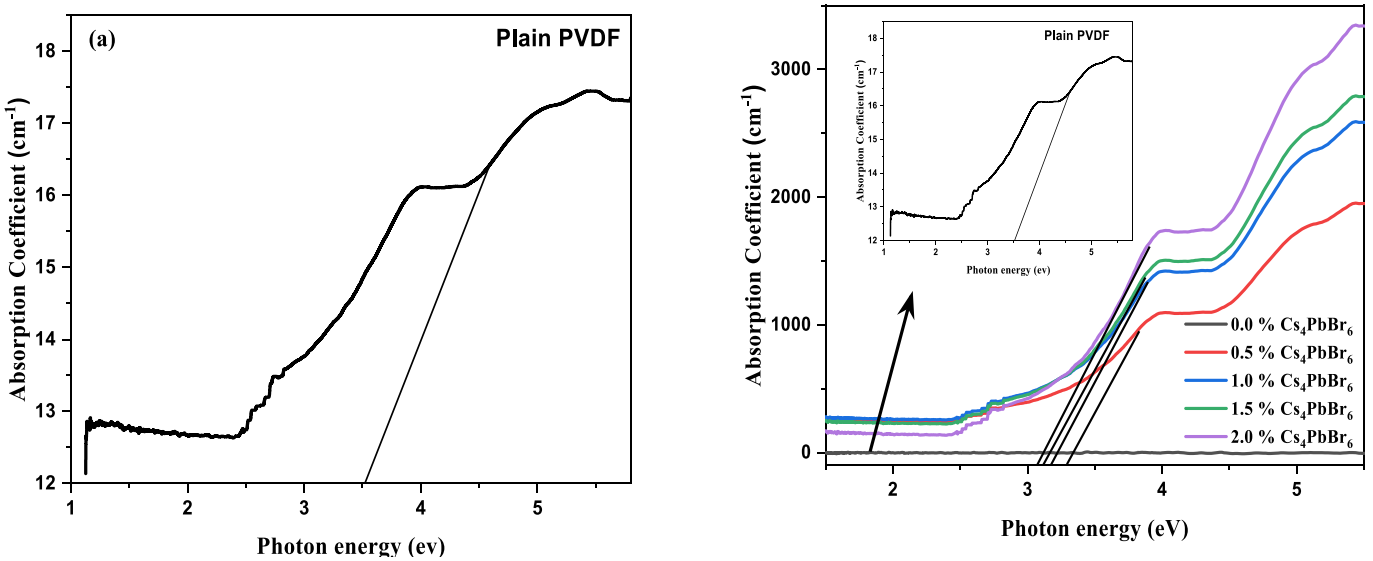

Fig. 9. Absorption co-efficient as a function of photon energy for the fabricated (a) plain PVDF (b) PVDF/Cs_4PbBr_6 nanocomposites.

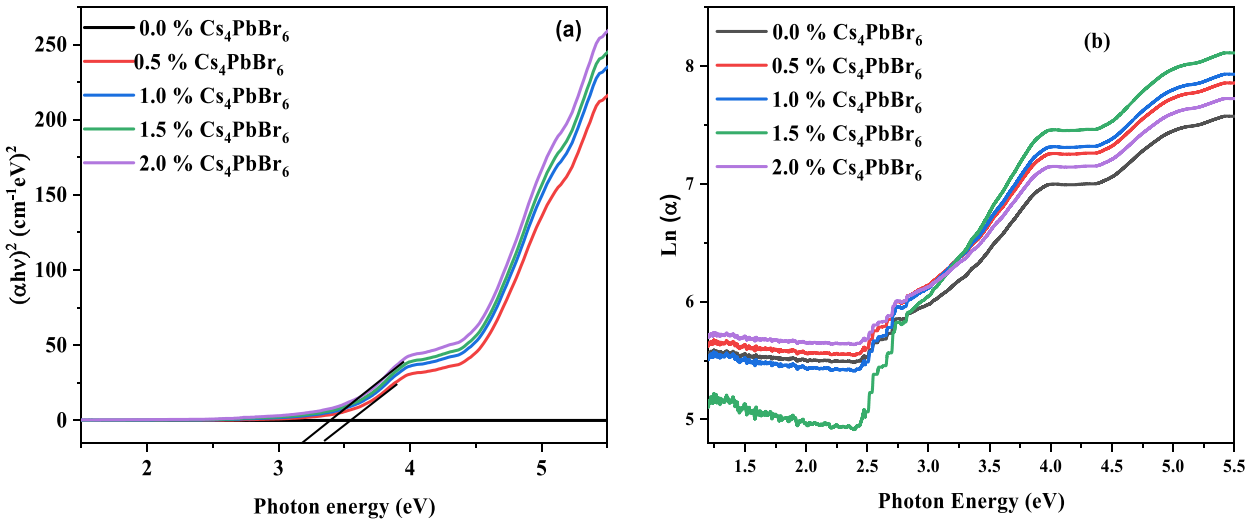

Fig. 10. Plots of (a) direct and (b) Urbach tail as a function of photon energy for pure PVDF and PVDF/Cs_4PbBr_6 nanocomposites.

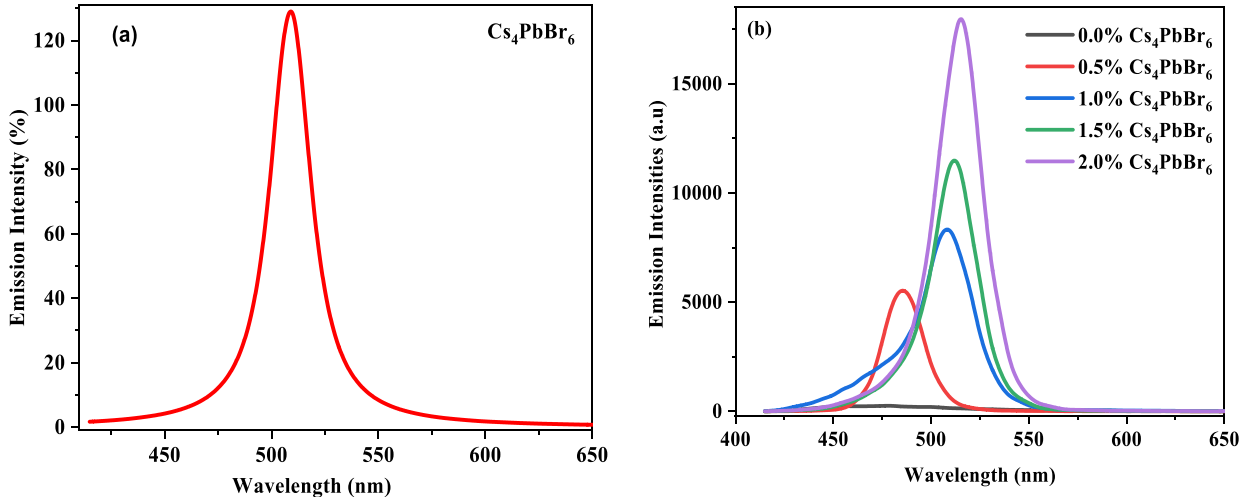

Fig. 11. Photoluminescence emission spectra of **(a)** Cs_4PbBr_6 **(b)** PVDF/Cs_4PbBr_6 nanocomposites.

bandgaps of 0D perovskites, which in turn causes the decoupling of the Pb-6 s, 6p, and Br-4p atomic orbitals. Despite their large bandgaps, 0D perovskites play a crucial role in boosting the PLQY of green emitters. This is accomplished by providing the appropriate dielectric media (molecular matrix) and transferring the energy of Pb^{2+} ion emission to the green emitting centers [31].

The synthesized PVDF/Cs_4PbBr_6 nanocomposites display dopant dependent photonic emission as a result of the Cs_4PbBr_6 nano filler-induced changes in the electronic band structure of PVDF nanocomposite films (as measured by changes in band gap). The results obtained are displayed in Fig. 11**(b)**. The PL spectra is recorded with the excitation wavelength of 370 nm whereas, the emission wavelength of the nanocomposites ranges 460–560 nm with varying λ_{max} with the concentration of the perovskite. Furthermore, from the PL spectra it is cleared that the prepared nanocomposites exhibit substantial Stock's shift of 130 nm owing to efficient photonic down conversion. The variation of the λ_{max} with the concentration of the perovskite is presented in the Table 4.

The optical and recombination losses made the current generation of solar modules/photovoltaic cells to decrease their quantum efficiencies, particularly in the shorter wavelength (400 nm) regimes Rothemund [52]. The incorporation of perovskite based Luminescent down converter (LDC) layers into photovoltaic cells is an attractive prospect. In this case, the added perovskite based LDC layers cause a UV to visible photonic down-conversion or photon cutting, which significantly reduces thermalization losses (Wang et al., 2018) [53]. Accordingly, PL emission studies in the current investigation show the fabricated nanocomposites inherent abilities to down-convert high-energy UV photons to relatively lower-energy visible light, thereby serving as effective LDC layers for photovoltaic applications. Fluorescence excitation/emission investigations, shows an excitation peak maximum approximately 3.85 eV/320 nm, in agreement with UV–Visible absorbance measurements, were used to optimize the energy needs for luminous transitions. While the fluorescence emission spectrum of PVDF/Cs_4PbBr_6 systems made with Cs_4PbBr_6 provides insight into the dopant-dependent photonic

Table 4
Photoluminescence properties of the Cs_4PbBr_6 and its PVDF nanocomposites.

Sl. No.	Cs_4PbBr_6/PVDF (wt/wt%)	PL emission (λ_{max})	$\tau_1 \pm 1.2$ (ns)
1	100/00	510	22.4
2	00/100	480	2.06
3	0.5/99.5	485	25.29
4	1.0/99.0	505	28.07
5	1.5/98.5	510	29.25
6	2.0/98.0	515	34.74

emission characteristics. In contrast to undoped PVDF films, which are non-fluorescent, the PVDF/Cs_4PbBr_6 NC films exhibit an extremely bright green emission (2.85–2.33 eV). Furthermore, when a semiconductor is introduced into a polymer matrix, most research on the light-emitting characteristics of semiconductor nanoparticles has often observed that the luminous centers are unintentionally destroyed [54,55], particularly when the polymeric host contains halogens. As a result, the fluorine backed pure PVDF films (in the current work) likewise continue to be non-fluorescent. In contrast, it is anticipated that the addition of Cs_4PbBr_6 nanofillers would cause the fluorine backboned PVDF to display charge transfer transitions with the perovskite fractals, which in turn will deactivate the fluorine group effectiveness in preventing luminescence and result in fluorescence emission.

Additionally, synergistic filler-matrix interactions may be responsible for the unique fluorescence emissions seen by PVDF/Cs_4PbBr_6 nanocomposites. These interactions may be able to significantly alter the electronic band structures, leading to the emergence of completely new material features. Additionally, the fluorescence spectrum investigations (excitation/emission) support the effective fluorescent emission-mediated down-conversion of PVDF/Cs_4PbBr_6 nanocomposites affected high energy UVA radiations (370 nm) to low energy visible light (485–515 nm) radiations. After the insertion of Cs_4PbBr_6 nanofiller, the new fluorescence emission properties of free-standing PVDF nanocomposites may be explained by using the popular processes suggested in the literature [56],Xiong [57].

These properties include intrinsic Pb^{2+} ion emission, large exciton binding energy, and small polaron formation upon photoexcitation, in addition to anomalous green PL with improved stability. This results in visible emission by the recombination of photo-generated charge carriers, present in perovskite with surface defect levels. The recombination of light-induced electrons (in/near the conduction band) is emphasized in one of the suggested methods, while photo-generated holes (in/near the valence band) are used to produce light emission in the other. A possible energy transfers between the PVDF and the inorganic nanofiller [31] involving the transition photo-generated electrons from the highest occupied molecular orbital (HOMO) of Cs_4PbBr_6 (the allowed optical transition from the excited state $^3P_1$ to the ground state $^1S_0$ of the Pb^{2+} ion and low energy band to charger transfer state (D-state) emission of the Pb^{2+} ion in the host lattice) valance band (VB) to the conduction band (CB) of PVDF is thought to be the cause of the green light emission observed by PVDF/Cs_4PbBr_6.

To elucidate the emission and photo physical properties of the obtained Cs_4PbBr_6 and its PVDF polymer nanocomposites were analyzed in liquid and solid phase respectively by using time resolved PL decay (TRPLD) and the results are computed in Table 4. Fig. 12 **(a)** and **(b)** shows the graph of PL lifetime decay for Cs_4PbBr_6 and its PVDF nanocomposites with varying concentration (0 to 2wt/wt%). Fig. 12**(a)** represents the TRPLD of the synthesized Cs_4PbBr_6 and after fitting this graph life time was found to 22.40 ± 1.2 ns which has 100 % greater value when compared to previous works (shows around 11–13 ns)[58]. To probe the effect of doping of perovskite into the PVDF host on life time decay of polymer TRPLD is employed and the graph is displayed in Fig. 12**(b)**. From the **Table** it is clear that with the increase in the concentration of the perovskite the PL life time decay also increases ranging from 2.06 to 34.74 ns indicating the monotonic increase with the concentration of the perovskite and also a concertation dependent phenomenon. This increase in the TRPLD of the nanocomposites may be attributed for the delayed exciton radiative recombination [59].

To study the effect of the perovskite concentration on the emission colour CIE chromaticity diagram (developed by the Commission Internationale de l'Eclairage) is employed. Furthermore, by mapping colors that are visible to the human eye in terms of hue and saturation, a CIE chromaticity diagram enables the comparison of the quality of colors. The CIE chromaticity diagram is drawn by using PL data and the result is presented in Fig. 13. It is clear that the composites shows an increase (red shift) in the emission wavelength ranges from 480 to 515 nm, i.e.

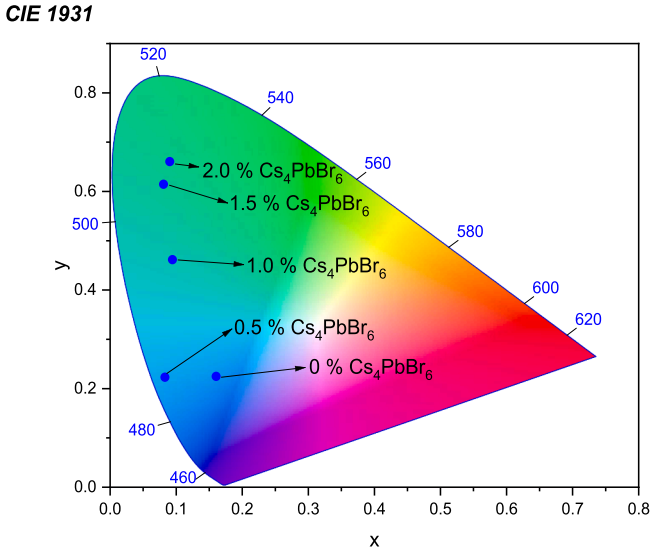

Fig. 13. Chromaticity CIE diagram for the prepared PVDF/Cs_4PbBr_6 nanocomposites.

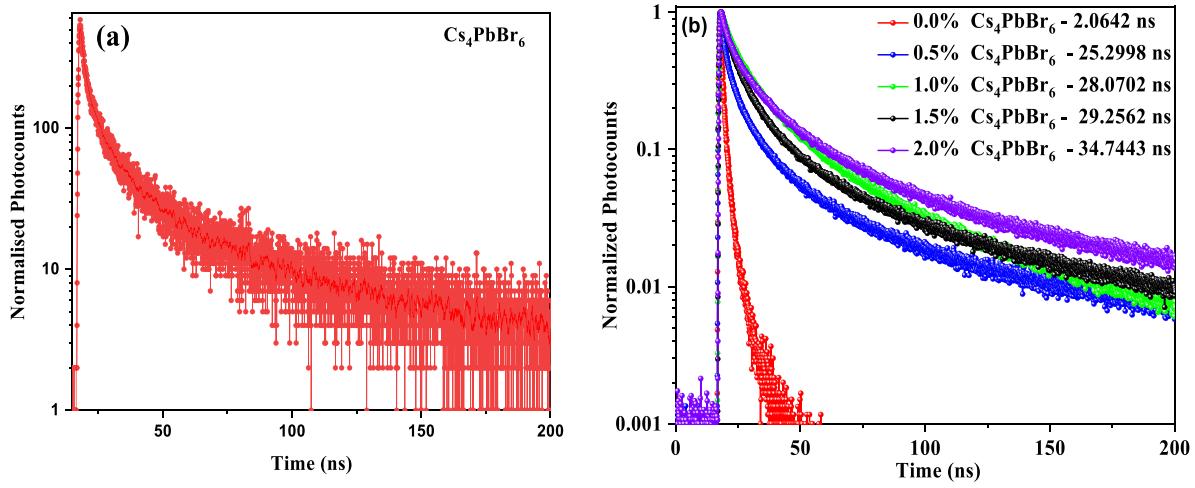

Fig. 12. Time resolved photoluminescence decay curve of (a) Cs_4PbBr_6 and (b) PVDF/Cs_4PbBr_6 nanocomposites.

emission colour change from blue to green with an increase in perovskite concentration from 0 to 2.0 wt/wt%. The comparision of the optical properties of the previous work has been tabulated in Table 5.

3.5. Wettability and surface energy studies

The critical feature of wetting is affected by the liquids used and the characteristics of the solid surface (hydrophobic or hydrophilic). Fig. 14 displays the results of a contact angle study of the wetting behavior of PVDF nanocomposites films doped with 0 %, 0. 5 %, 1.0 %, 1.5 %, and 2.0 % Cs_4PbBr_6. The contact angle of pure PVDF is 61.46° degrees, which demonstrates its wettability. From Table 6 it is clear that as the contact angle increases, surface energy decreases, the decrease in attractive cohesive force that sinks and spreads the water droplet. Consistent with prior results, water droplets with hemispheric meniscus morphologies of 71.28°, 73.79°, 77.93°, and 80.22° were formed when 0.5, 1.0, 1.5, and 2 % Cs_4PbBr_6 were incorporated into the PVDF matrix. In spite of being less wettable than pure PVDF, this contact angle discovery implies that PVDF nanocomposites are nonetheless wettable [60]. There is less of a barrier between nanocomposites and water droplets than there is with pure PVDF. Nanocomposites have lower surface energy and interfacial tension because of the increased contact angle. Furthermore, to probe the water stability of the prepared nanocomposites water immersion test is conducted (**Fig. S8**). The test conducted by immersing prepared nanocomposites in water for 60 days and observing their luminescence in UV-light. From the results it is cleared that the PVDF/Cs_4PbBr_6 nanocomposites are exhibiting greater stability to water without losing its luminescence property even after 60 days.

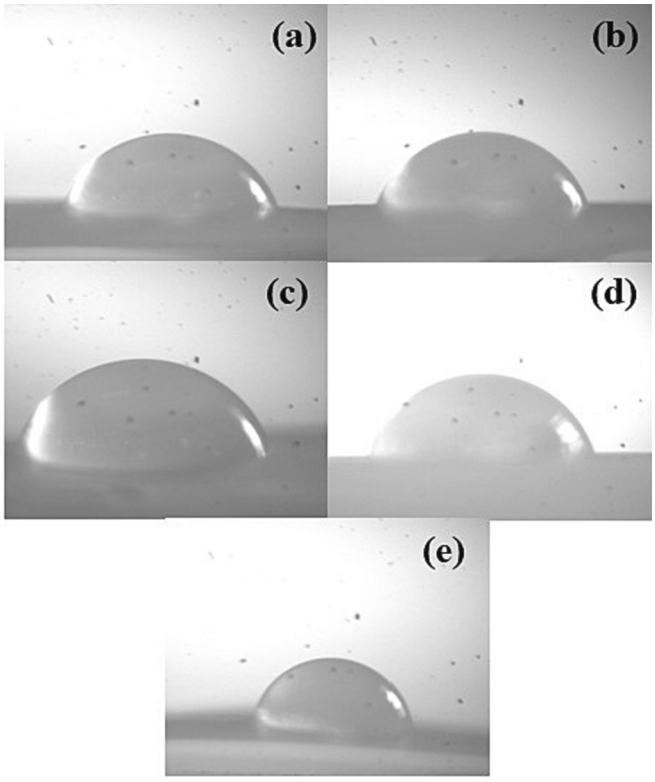

Fig. 14. Images of water contact angle of Cs_4PbBr_6/PVDF nanocomposites.

4. Conclusion

In this present work, we successfully synthesized the Cs_4PbBr_6 by the re-precipitation method and fabricated its PVDF nanocomposites *via* the solvent casting method with different concentrations of Cs_4PbBr_6. From the XRD rhombohedral unit cell of the crystal lattice, TEM with SAED confirms the prepared Cs_4PbBr_6 is nanoscale and is single phase, further, UV–Visible and PL spectroscopy results show the absorbance at 310 nm and emission spectra at 510 nm with the narrow FWHM of 22 nm, confirming the existence of Cs_4PbBr_6 with a TRPLD of 22 ns. From SEM analysis, we witnessed that prepared Cs_4PbBr_6 nanoparticles are uniformly distributed in PVDF matrix with different concentrations, viz. 0.0, 0.5, 1.0, 1.5, and 2.0 wt/wt%. WAXS studies of the nanocomposites clearly indicated that there is a strong interaction between the polymer and Cs_4PbBr_6 which affects the microcrystalline properties of the polymer. From the UV–Visible spectra of the nanocomposites, it is clear that the nanocomposites have a strong absorption band at 280–320 nm (UV-B), with $\lambda_{max} = 310$ nm, indicating that the absorbance of Cs_4PbBr_6 is protected and it is encapsulated in PVDF, which has applications in UV-shielding or UV-blocking in the UV-B region of UV radiation. Optical parameters it was found that the nanocomposites undergo direct type transitions. The PL spectral reveals that the emission varies from 485 to 515 nm as the concentration varies from 0.0 − 2.0 wt/wt% indicating the red shift. Additionally, the nanocomposites exhibit shocks shift of ≈115 nm indicating down conversion. The TRPLD of the prepared Cs_4PbBr_6 and Cs_4PbBr_6@PVDF nanocomposites showed greater life time decay, which makes them a suitable candidate for light emitting diodes and photovoltaic applications. The water contact angle and water immersion test show greater stability of the prepared Cs_4PbBr_6 and its PVDF nanocomposites, which makes them suitable for outdoor applications such as display devices and photovoltaics. In summary, we conclude that the synthesized Cs_4PbBr_6 and its PVDF nanocomposites

Table 6
Comparison of optical properties with previous works.

PVDF/Cs_4PbBr_6 (wt/wt %)	Contact Angle (°) ± 0.5	Surface Energy (N/m) ± 1.0
100/00	61.46	101.87
99.5/0.5	71.28	96.16
99.0/1.0	73.79	93.17
98.5/1.5	77.93	88.02
98/2.0	80.22	85.16

Table 5
The obtained data of the wettability of PVDF/Cs_4PbBr_6 nanocomposites.

Sl. No	Perovskite/polymer nanocomposites	Absorbance (nm)	PL emission wavelength (nm)	Time resolved PL decay (ns)	Reference
1	Cs4PbBr$_6$/Poly [2-methoxy-5-(2-ethyl-hexyloxy)-1,4-phenylene-vinylene]	–	580	–	Al-Asbahi et al. [61]
2	Cs4PbBr$_6$/CsPbBr$_3$/ PMMA	318	512	55	Li et al. [62]
3	CsPbBr3/poly(styrene-ethylene-butylene-styrene	500	520	30.5	Raja, S. N., et al., [17]
4	CsPbBr$_3$/PMMA	–	515	30.8	Ma, K., et al., [27]
5	MAPbBr$_3$/PMMA	–	521	60	Li, X., et al., [7]
6	MAPbBr$_3$/PMMA or MMA	515	521	16,	Y. Xin et al., [63]
	MAPbBr$_3$/BMA	539	522	25.6	
7	Cs_4PbBr_6/PVDF	310	510–525	34.77	This work

with enhanced stability can widen their application in outdoor opto-electronics and are a suitable candidate for industrial applications.

CRediT authorship contribution statement

Nagappa Shivaprasad: Methodology, Original draft preparation. **Mysore Guruswamy Veena:** Editing, reviewing and supervision. **Beejaganahalli Sangameshwara Madhukar:** Conceptualization, Investigation, Supervision. **Rajanna Kavya:** Formal analysis, Software. **K. Sarath:** Project administration. **Pradeep Reddy Vanga:** Guidance. **Geoge Sahaya Dennish Babu:** Draft Editing. **Bhagyashree Mahesha Sachith:** Conduct. **Anjanapura Venkatarmanaiah Raghu:** Project administration, Supervision.

Declaration of Competing Interest

The authors declare the following financial interests/personal relationships which may be considered as potential competing interests: [I am author and corresponding author and this work never published before and this is a new work].

Data availability

Data will be made available on request.

Appendix A. Supplementary data

Supplementary data to this article can be found online at https://doi.org/10.1016/j.inoche.2023.111761.

References

[1] J.S. Manser, M.I. Saidaminov, J.A. Christians, O.M. Bakr, P.V. Kamat, Making and breaking of lead halide perovskites, Acc. Chem. Res. 49 (2) (2016) 330–338, https://doi.org/10.1021/acs.accounts.5b00455.

[2] Q.A. Akkerman, A.L. Abdelhady, L. Manna, Zero-dimensional cesium lead halides: History, properties, and challenges, The J. Phys. Chem. Letters. 9 (9) (2018) 2326–2337, https://doi.org/10.1021/acs.jpclett.8b00572.

[3] Z. Bao, H.C. Wang, Z.F. Jiang, R.J. Chung, R.S. Liu, Continuous synthesis of highly stable Cs4PbBr 6 perovskite microcrystals by a microfluidic system and their application in white-light-emitting diodes, Inorganic Chem. 57 (21) (2018) 13071–13074, https://doi.org/10.1021/acs.inorgchem.8b01985.

[4] G. Murugadoss, R. Thangamuthu, S.M.S. Kumar, N. Anandhan, M.R. Kumar, A. Rathishkumar, Synthesis of ligand-free, large scale with high quality all-inorganic CsPbI3 and CsPb2Br 5 nanocrystals and fabrication of all-inorganic perovskite solar cells, J. Alloys and Compounds. 787 (2019) 17–26, https://doi.org/10.1016/j.jallcom.2019.02.018.

[5] G. Murugadoss, S. Tanaka, G. Mizuta, S. Kanaya, H. Nishino, T. Umeyama, S. Ito, Light stability tests of methylammonium and formamidinium Pb-halide perovskites for solar cell applications, Japanese J. Applied Phy. 54 (8S1) (2015) 08KF08, https://doi.org/10.7567/JJAP.54.08KF08.

[6] G. Murugadoss, R. Thangamuthu, S.M.S. Kumar, Fabrication of $CH_3NH_3PbI_3$ perovskite-based solar cells: Developing various new solvents for CuSCN hole transport material, Solar Energ. Materials and Solar Cells. 164 (2017) 56–62, https://doi.org/10.1016/j.solmat.2017.02.011.

[7] X. Li, Z. Xue, D. Luo, C. Huang, L. Liu, X. Qiao, T. Wang, A stable lead halide perovskite nanocrystals protected by PMMA, Sci. China Mater. 61 (3) (2018) 363–370, https://doi.org/10.1007/s40843-017-9148-7.

[8] J.S. Chen, T.L. Doane, M. Li, H. Zang, M.M. Maye, M. Cotlet, 0D–2D and 1D–2D semiconductor hybrids composed of all inorganic perovskite nanocrystals and single-layer graphene with improved light harvesting, Part. Part. Syst. Char. 35 (2) (2018) 1700310, https://doi.org/10.1002/ppsc.201700310.

[9] S. Demchyshyn, J.M. Roemer, H. Groiß, H. Heilbrunner, C. Ulbricht, D. Apaydin, M. Kaltenbrunner, Confining metal-halide perovskites in nanoporous thin films, Sci. Advances. 3 (8) (2017), https://doi.org/10.1126/sciadv.1700738.

[10] M. Meyns, M. Perálvarez, A. Heuer-Jungemann, W. Hertog, M. Ibáñez, R. Nafria, A. G. Kanaras, Polymer-enhanced stability of inorganic perovskite nanocrystals and their application in color conversion LEDs, ACS Appl. Mater. Interfaces. 8 (30) (2016) 19579–19586, https://doi.org/10.1021/acsami.6b02529.

[11] M.T. Ramesan, T. Anjitha, K. Parvathi, T. Anilkumar, G. Mathew, Nano zinc ferrite filler incorporated polyindole/poly (vinyl alcohol) blend: Preparation, characterization, and investigation of electrical properties, Advances in Polymer Techno. 37 (8) (2018) 3639–3649, https://doi.org/10.1002/adv.22148.

[12] S. Sankar, A.A. Naik, T. Anilkumar, M.T. Ramesan, Characterization, conductivity studies, dielectric properties, and gas sensing performance of in situ polymerized polyindole/copper alumina nanocomposites, J. Applied Polymer Sci. 137 (38) (2020) 49145, https://doi.org/10.1002/app.49145.

[13] M.T. Ramesan, K.P. Greeshma, K. Parvathi, T. Anilkumar, Structural, electrical, thermal, and gas sensing properties of new conductive blend nanocomposites based on polypyrrole/phenothiazine/silver-doped zinc oxide, J. Vinyl and Additive Techno. 26 (2) (2020) 187–195, https://doi.org/10.1002/vnl.21732.

[14] M.T. Ramesan, V. Nidhisha, P. Jayakrishnan, Facile synthesis, characterization and material properties of a novel poly (vinyl cinnamate)/nickel oxide nanocomposite, Polym. Int.. 66 (4) (2017) 548–556, https://doi.org/10.1002/pi.5288.

[15] M.T. Ramesan, V. Nidhisha, P. Jayakrishnan, Synthesis, characterization and conducting properties of novel poly (vinyl cinnamate)/zinc oxide nanocomposites via in situ polymerization, Materials Sci. in Semiconductor Processing. 63 (2017) 253–260, https://doi.org/10.1016/j.mssp.2017.02.027.

[16] J. Shamsi, A.S. Urban, M. Imran, L. De Trizio, L. Manna, Metal halide perovskite nanocrystals: Synthesis, post-synthesis modifications, and their optical properties, Chem. Rev.. 119 (5) (2019) 3296–3348, https://doi.org/10.1021/acs.chemrev.8b00644.

[17] S.N. Raja, Y. Bekenstein, M.A. Koc, S. Fischer, D. Zhang, L. Lin, A.P. Alivisatos, Encapsulation of perovskite nanocrystals into macroscale polymer matrices: Enhanced stability and polarization, ACS Appl. Mater. Interfaces. 8 (51) (2016) 35523–35533, https://doi.org/10.1021/acsami.6b09443.

[18] Z. Wang, L. Tan, X. Pan, G. Liu, Y. He, W. Jin, H. Gu, Self-powered viscosity and pressure sensing in microfluidic systems based on the piezoelectric energy harvesting of flowing droplets, ACS Appl. Mater. Interfaces. 9 (34) (2017) 28586–28595, https://doi.org/10.1021/acsami.7b08541.

[19] S. Alhassan, M. Alshammari, K. Alshammari, T. Alotaibi, A.H. Alshammari, Y. Fawaz, T.A.M. Taha, M. Henini, Preparation and optical properties of PVDF-CaFe2O4 polymer nanocomposite films, Polymers 15 (2023) 2232, https://doi.org/10.3390/polym15092232.

[20] S. Alhassan, K. Alshammari, M. Alshammari, T. Alotaibi, A.H. Alshammari, Y. Fawaz, M. Henini, Synthesis and optical properties of polyvinylidene difluoride nanocomposites comprising MoO_3/g-C_3N_4, Results in Phy. 48 (2023) 106403, https://doi.org/10.1016/j.rinp.2023.106403.

[21] T.A. Taha, M.H. Mahmoud, Synthesis and characterization of PVDF-Er_2O_3 polymer nanocomposites for energy storage applications, Materials Chem. and Phy. 270 (2021) 124827, https://doi.org/10.1016/j.matchemphys.2021.124827.

[22] T.A. Taha, M.H. Mahmoud, H.H. Hamdeh, Development, thermal and dielectric investigations of PVDF-Y_2O_3 polymer nanocomposite films, J. Polymer Research. 28 (2021) 1–9, https://doi.org/10.1007/s10965-021-02508-y.

[23] A.J. Lovinger, Ferroelectric polymers Sci. 220 (4602) (1983) 1115–1121, https://doi.org/10.1126/science.220.4602.1115.

[24] Y.L. Liu, Y. Li, J.T. Xu, Z.Q. Fan, Cooperative effect of electrospinning and nanoclay on formation of polar crystalline phases in poly (vinylidene fluoride), ACS Appl. Mater. Interfaces. 2 (6) (2010) 1759–1768, https://doi.org/10.1021/am1002525.

[25] J. He, H. Chen, H. Chen, Y. Wang, S.T. Wu, Y. Dong, Hybrid downconverters with green perovskite-polymer composite films for wide color gamut displays, Opt. Express. 25 (11) (2017) 2915–12925, https://doi.org/10.1364/OE.25.012915.

[26] S. Hou, Y. Guo, Y. Tang, Q. Quan, Synthesis and stabilization of colloidal perovskite nanocrystals by multidentate polymer micelles, ACS Appl. Mater. Interfaces. 9 (22) (2017) 18417–18422, https://doi.org/10.1021/acsami.7b03445.

[27] K. Ma, X.Y. Du, Y.W. Zhang, S. Chen, In situ fabrication of halide perovskite nanocrystals embedded in polymer composites *via* microfluidic spinning microreactors, J. Materials Chem. C. 5 (36) (2017) 9398–9404, https://doi.org/10.1039/C7TC02847D.

[28] L. Xi, C.B. Boothroyd, T. Salim, S. Borghardt, Y.M. Lam, B.E. Kardynał, Facile in situ synthesis of stable luminescent organic–inorganic lead halide perovskite nanoparticles in a polymer matrix, J. Materials Chem. C. 5 (29) (2017) 7207–7214, https://doi.org/10.1039/c7tc02109g.

[29] H. An, W.K. Kim, C. Wu, T.W. Kim, Highly-stable memristive devices based on poly (methylmethacrylate): CsPbCl3 perovskite quantum dot hybrid nanocomposites, Org. Electron.. 56 (2018) 41–45, https://doi.org/10.1016/j.orgel.2018.02.001.

[30] S. Seth, A. Samanta, Fluorescent phase-pure zero-dimensional perovskite-related Cs4PbBr 6 microdisks: Synthesis and single-particle imaging study, The J. Phys. Chem. Letters. 8 (18) (2017) 4461–4467, https://doi.org/10.1021/acs.jpclett.7b02100.

[31] J. Almutlaq, J. Yin, O.F. Mohammed, O.M. Bakr, The benefit and challenges of zero-dimensional perovskites, The J. Phys. Chem. Letters. 9 (14) (2018) 4131–4138, https://doi.org/10.1021/acs.jpclett.8b00532.

[32] T. Wu, B. Zhou, T. Zhu, J. Shi, Z. Xu, C. Hu, J. Wang, Facile and low-cost approach towards a PVDF ultrafiltration membrane with enhanced hydrophilicity and antifouling performance *via* graphene oxide/water-bath coagulation, RSC Adv. 5 (11) (2015) 7880–7889, https://doi.org/10.1039/C4RA13476A.

[33] T.E. Somesh, M.Q. Al-Gunaid, B.S. Madhukar, Siddaramaiah, Photosensitization of optical band gap modified polyvinyl alcohol films with hybrid $AgAlO_2$ nanoparticles, J. Materials Sci.: Materials in Electronics 30 (2019) 37–49, https://doi.org/10.1007/s10854-018-0226-3.

[34] L. Wang, H. Liu, Y. Zhang, O.F. Mohammed, Photoluminescence origin of zero-dimensional Cs4PbBr 6 perovskite, ACS Energy Lett.. 5 (1) (2019) 87–99, https://doi.org/10.1021/acsenergylett.9b02275.

[35] S.H. Choi, B.Y. Kim, B.K. Kang, S.B. Kwon, H.J. Jeong, G.S. Han, Y.H. Song, Innovative rapid synthesis design of water-stable solid-state Cs4PbBr 6 perovskite luminescence materials for next generation display technology, Applied Surface Sci. 542 (2021) 148696, https://doi.org/10.1016/j.apsusc.2020.148696.

[36] Z. Liu, Y. Bekenstein, X. Ye, S.C. Nguyen, J. Swabeck, D. Zhang, A.P. Alivisatos, Ligand mediated transformation of cesium lead bromide perovskite nanocrystals to

lead depleted Cs4PbBr 6 nanocrystals, J. the American Chemical Society. 139 (15) (2017) 5309–5312, https://doi.org/10.1021/jacs.7b01409.
[37] I.H. Kim, D.H. Baik, Y.G. Jeong, Structures, electrical, and dielectric properties of PVDF-based nanocomposite films reinforced with neat multi-walled carbon nanotube, Macromol. Res.. 20 (2012) 920–927, https://doi.org/10.1007/s13233-012-0064-8.
[38] S. Pang, Y. Hernandez, X. Feng, K. Müllen, Graphene as transparent electrode material for organic electronics, Adv. Mater. 23 (25) (2011) 2779–2795, https://doi.org/10.1002/adma.201100304.
[39] S. El-Sayed, Optical properties and dielectric relaxation of polyvinylidene fluoride thin films doped with gadolinium chloride, Phys. B Condens. Matter. 454 (2014) 197–203, https://doi.org/10.1016/j.physb.2014.07.076.
[40] S. Schneider, X. Drujon, J.C. Wittmann, B. Lotz, Impact of nucleating agents of PVDF on the crystallization of PVDF/PMMA blends, Polymer 42 (21) (2001) 8799–8806, https://doi.org/10.1016/S0032-3861(01)00349-4.
[41] H.S. Vedhavathi, U.S. Divya, B.S. Madhukar, P.R. Vanga, N.K. Swamy, PVA/Gd_2O_3@ Zno nanocomposite films as new Uv-blockers: Structure and optical revelations, J. Inorganic and Organometallic Polymers and Materials. 32 (5) (2022) 1853–1867, https://doi.org/10.1007/s10904-022-02231-1.
[42] B.R. Ali, F. Kadhem, Study of the optical properties and optical band gap for the coumarine–102/PMMA thin films, Int. J. Appl. Innov. Eng. Manage. 2 (2013) 564–571.
[43] J. Tauc Chap. 5 of "Optical Properties of Solids" ed. By F. Abeles. 1972.
[44] I.S. Elashmawi, E.M. Abdelrazek, H.M. Ragab, N.A. Hakeem, Structural, optical and dielectric behavior of PVDF films filled with different concentrations of iodine, Phys. B Condens. Matter. 405 (1) (2010) 94–98, https://doi.org/10.1016/j.physb.2009.08.037.
[45] A.S. Roy, S. Gupta, S. Sindhu, A. Parveen, P.C. Ramamurthy, Dielectric properties of novel PVA/ZnO hybrid nanocomposite films, Composites Part B: Eng. 47 (2013) 314–319, https://doi.org/10.1016/j.compositesb.2012.10.029.
[46] S.M. Qaid, H.M. Ghaithan, B.A. Al-Asbahi, A.S. Aldwayyan, Investigation of the surface passivation effect on the optical properties of CsPbBr 3 perovskite quantum dots, Surf. Interfaces. 23 (2021) 100948, https://doi.org/10.1016/j.surfin.2021.100948.
[47] F. Urbach, The long-wavelength edge of photographic sensitivity and of the electronic absorption of solids, Phys. Rev. 92 (5) (1953) 1324, https://doi.org/10.1103/PhysRev.92.1324.
[48] G. Santhosh, B.S. Madhukar, G.P. Nayaka, B. Siddaramaiah, Luminescent down-shifting aluminosilicate nanocomposites: An efficient UVA shielding material for photovoltaics, J. Materials Sci: Materials in Electronics 29 (2018) 6720–6729, https://doi.org/10.1007/s10854-018-8658-3.
[49] M. Ma, F.W. Mont, X. Yan, J. Cho, E.F. Schubert, G.B. Kim, C. Sone, Effects of the refractive index of the encapsulant on the light-extraction efficiency of light-emitting diodes, Opt. Express. 19 (105) (2011) A1135–A1140, https://doi.org/10.1364/OE.19.0A1135.
[50] N. Kundachira Subramani, Opto-electrical characteristics of poly (vinyl alcohol)/cesium zincate nanodielectrics, The J. Phy. Chem. C 119 (35) (2015) 20244–20255, https://doi.org/10.1021/acs.jpcc.5b03652.
[51] H. Zhang, Q. Liao, Y. Wu, J. Chen, Q. Gao, H. Fu, Pure zero-dimensional Cs4PbBr 6 single crystal rhombohedral microdisks with high luminescence and stability, Phy. Chem. Chemical Phy. 19 (43) (2017) 29092–29098, https://doi.org/10.1039/C7CP06097A.
[52] R. Rothemund, Optical modelling of the external quantum efficiency of solar cells with luminescent down-shifting layers, Sol. Energy Mater. Sol. Cells 120 (2014) 616–621, https://doi.org/10.1016/j.solmat.2013.10.004.
[53] H.Q. Wang, M. Batentschuk, A. Osvet, L. Pinna, C.J. Brabec, Rare-earth ion doped up-conversion materials for photovoltaic applications, Adv. Mater. 23 (22–23) (2011) 2675–2680, https://doi.org/10.1002/adma.201100511.
[54] S. Li, M. Meng Lin, M.S. Toprak, D.K. Kim, M. Muhammed, Nanocomposites of polymer and inorganic nanoparticles for optical and magnetic applications, Nano Reviews. 1 (1) (2010) 5214, https://doi.org/10.3402/nano.v1i0.5214.
[55] G.R. Suma, N.K. Subramani, K.N. Shilpa, S. Sachhidananda, S.V. Satyanarayana, Effect of Ce0.5 Zr0.5 O2 nano fillers on structural and optical behaviors of poly (vinyl alcohol), J. Materials Sci: Materials in Electronics. 28 (2017) 10707–10714, https://doi.org/10.1007/s10854-017-6846-1.
[56] A. Van Dijken, E.A. Meulenkamp, D. Vanmaekelbergh, A. Meijerink, The luminescence of nanocrystalline ZnO particles: The mechanism of the ultraviolet and visible emission, J. Luminescence 87 (2000) 454–456, https://doi.org/10.1016/S0022-2313(99)00482-2.
[57] H.M. Xiong, Photoluminescent ZnO nanoparticles modified by polymers, J. Materials Chem. 20 (21) (2010) 4251–4262, https://doi.org/10.1039/B918413A.
[58] L. Protesescu, S. Yakunin, M.I. Bodnarchuk, F. Krieg, R. Caputo, C.H. Hendon, M. V. Kovalenko, Nanocrystals of cesium lead halide perovskites (CsPbX3, X= Cl, Br, and I): Novel optoelectronic materials showing bright emission with wide color gamut, Nano Lett.. 15 (6) (2015) 3692–3696, https://doi.org/10.1021/nl5048779.
[59] B.M. Sachith, T. Okamoto, S. Ghimire, T. Umeyama, Y. Takano, H. Imahori, V. Biju, Long-range interfacial charge carrier trapping in halide perovskite-C60 and halide perovskite-TiO2 donor-acceptor films, The J. Phy. Chem. Letters. 12 (35) (2021) 8644–8651, https://doi.org/10.1021/acs.jpclett.1c01909.
[60] M.A. Bahattab, J. Donate-Robles, V. García-Pacios, J.M. Martín-Martínez, Characterization of polyurethane adhesives containing nanosilicas of different particle size, Inter. J. Adhesion and Adhesives. 31 (2) (2011) 97–103, https://doi.org/10.1016/j.ijadhadh.2010.11.001.
[61] B.A. Al-Asbahi, S.M. Qaid, A.S. Aldwayyan, Effect of donor-acceptor concentration ratios on non-radiative energy transfer in zero-dimensional Cs4PbBr 6 perovskite/meh-ppv nanocomposite thin films, Polymers 12 (2) (2020) 444.
[62] X. Li, Z. Wen, S. Ding, F. Fang, B. Xu, J. Sun, X.W. Sun, Facile in situ fabrication of Cs4PbBr 6/CsPbBr3 nanocomposite containing polymer films for ultrawide color gamut displays, Adv. Optical Materials. 8 (13) (2020) 2000232, https://doi.org/10.1002/adom.202000232.
[63] Y. Xin, H. Zhao, J. Zhang, Highly stable and luminescent perovskite-polymer composites from a convenient and universal strategy, ACS Appl. Mater. Interfaces. 10 (2018) 4971–4980, https://doi.org/10.1021/acsami.7b16442.